Journal of Biotechnology 363 (2023) 19–31

Contents lists available at ScienceDirect

Journal of Biotechnology

journal homepage: www.elsevier.com/locate/jbiotec

Research article

Biochemical monitoring throughout all stages of rabies virus-like particles production by Raman spectroscopy using global models

Luis Giovani Oliveira Guardalini [a], Paulo Eduardo da Silva Cavalcante [a], Jaci Leme [a], Renata Gois de Mello [a], Thaissa Consoni Bernardino [a], Renato Mancini Astray [b], Eduardo Barbosa [c], Suellen Regina da Silveira [c], Paulo Lee Ho [d], Aldo Tonso [e], Soraia Attie Calil Jorge [a], Eutimio Gustavo Fernández Núñez [f,*]

[a] Laboratório de Biotecnologia Viral, Instituto Butantan, Av Vital Brasil 1500, São Paulo, CEP 05503-900 São Paulo, SP, Brazil
[b] Laboratório Multipropósito, Instituto Butantan, Av. Vital Brasil 1500, São Paulo, CEP 05503-900 São Paulo, SP, Brazil
[c] Pensalab, Rua Minerva, 129 – Perdizes, São Paulo, CEP 05007-030 São Paulo, SP, Brazil
[d] Centro Bioindustrial, Instituto Butantan, Av. Vital Brasil 1500, São Paulo, CEP 05503-900 São Paulo, SP, Brazil
[e] Laboratório de Células Animais, Departamento de Engenharia Química, Escola Politécnica, Universidade de São Paulo. Av. Prof. Luciano Gualberto, trav. 3, 380, 05508-900 São Paulo, SP, Brazil
[f] Laboratório de Engenharia de Bioprocessos. Escola de Artes, Ciências e Humanidades (EACH), Universidade de São Paulo, Rua Arlindo Béttio, 1000, CEP 03828-000, São Paulo, SP, Brazil

ARTICLE INFO

Keywords:
Spodoptera frugiperda (Sf9)
Virus-like particles
Raman spectroscopy
Rabies virus
Bioprocess monitoring

ABSTRACT

This work aimed to quantify growth and biochemical parameters (viable cell density, Xv; cell viability, CV; glucose, lactate, glutamine, glutamate, ammonium, and potassium concentrations) in upstream stages to obtain rabies virus-like particles (rabies VLP) from insect cell-baculovirus system using on-line and off-line Raman spectra to calibrate global models with minimal experimental data. Five cultivations in bioreactor were performed. The first one comprised the growth of uninfected *Spodoptera frugiperda* (Sf9) cells, the second and third runs to obtain recombinant baculovirus (rBV) bearing Rabies G glycoprotein and matrix protein, respectively. The fourth one involved the generation of rabies VLP from rBVs and the last one was a repetition of the third one with cell inoculum infected by rBV. The spectra were acquired through a Raman spectrometer with a 785-nm laser source. The fitted Partial Least Square models for nutrients and metabolites were comparable with those previously reported for mammalian cell lines (Relative error < 15 %). However, the use of this chemometrics approach for Xv and CV was not as accurate as it was for other parameters. The findings from this work established the basis for bioprocess Raman spectroscopical monitoring using insect cells for VLP manufacturing, which are gaining ground in the pharmaceutical industry.

1. Introduction

Rabies is a widespread viral zoonosis that affect wild, and domestic animals as well as humans. Every year, about 60,000 people die of rabies worldwide (Riccardi et al., 2021). Rabies prevention is effectively attained by vaccination in pre-exposure to rabies virus, or by vaccination and serum therapy in post-exposure treatment protocol. Most of the current rabies vaccines on the international market are obtained in cell culture or chicken embryos. The main cell substrate for rabies vaccine is from mammalian sources, including human diploid cells, rhesus monkey diploid embryo cells, African green monkey kidney cells (Vero), and baby hamster kidney fibroblasts (BHK21). Novel approaches under assessment for rabies vaccines comprise different hosts such as bacteria, insect cells and plants as well as RNA and DNA vaccines (Fooks et al., 2019; Moraes et al., 2012; Starodubova et al., 2015).

Many therapeutic recombinant proteins need to preserve the post-translational modifications (e.g., O-linked, and N-linked glycosylation, phosphorylation), protein folding in their native state and trafficking pathways. Therefore, it is vital in some cases that the post-translational pattern is correct to guarantee suitable solubility, stability, bioavailability for appropriate recognition and processing by the immune system of the patient (Orphanou and Gervais, 2018). Specifically, insect

* Corresponding author.
E-mail address: egfnunez@usp.br (E.G. Fernández Núñez).

https://doi.org/10.1016/j.jbiotec.2022.12.009
Received 25 September 2022; Accepted 27 December 2022
Available online 29 December 2022

Table 1
Spectra filtering approaches applied to the raw Raman spectral data before the PLS modeling.

Spectra filtering approach	Raw data	Smoothing	Baseline correction		Normalization	Others				
		Savitzky-Golay[a]	Lowest offset[b]	Row-center[c]	SNV[d]	MSC[e]	Derivates[f]			
							1st-quadratic	1st-cubic	2nd-cubic	3rd-quartic
1	X									
2			X		X	X				
3			X		X		X			
4			X		X			X		
5			X		X				X	
6			X		X					X
7				X	X	X				
8		X	X		X	X				
9		X		X	X	X				
10			X		X					

[a] Smoothing Savitzky-Golay removes noise by application a moving polynomial to the data (In this work was used a quadratic polynomial order with 15 points in each sub-model)
[b] Lowest offset baseline correction shifts each spectrum so that the lowest intensity of the spectrum is set to 0.
[c] Row-center baseline correction shifts each spectrum by subtracting the row mean from each row value.
[d] Normalization by Standard Normal Variate (SNV): each spectrum is normalized by subtracting the mean and dividing with standard deviation.
[e] Multiplicative signal correction (MSC): each spectrum is normalized by regressing it against the average spectrum over a selected set of spectra.
[f] Derivates is a method for reducing scatter effects for continuous spectra. In this work were considered the first, second and third derivates. The polynomial order is specified in the table. The points number in each sub-model was 15 and the distance between each point was 1.

cell-based recombinant protein manufacturing systems represents a mid-point between bacterial and mammalian expression systems. Its disadvantage with respect to mammalian cells is that it does not preserve the same glycosylation pattern, specifically, the N-linked glycosylation in insect cells is much simpler, restricted to small high mannose structures unless the host has been modified with additional enzymes (McKenzie and Abbott, 2018). The main advantage of insect cells lies on they are less demanding in terms of culture media and operating conditions. They also grow to higher densities compared to mammalian cells. This animal cell expression system has been used to manufacture at commercial scale Cervarix®, a GSK vaccine against cancers caused by human papillomavirus and Flublock®, an Influenza vaccine (Kesik--Brodacka, 2018; Moleirinho et al., 2020b).

On the other hand, virus-like particles (VLP) are proteins capable to form nanostructures resembling virus particles with potential applications against several diseases such as viral and bacterial infections, cancer, neurodegenerative and autoimmune disorders. As a rule, they are designed to trigger an immune response by presenting antigen on their surface. VLPs are assemblies of one or several types of virus protein forming a higher order structure, they can also contain a lipid outer envelope (Fuenmayor et al., 2017; Rüdt et al., 2019). Their biosafety in use and manufacturing is higher than classic virus vaccines due to the VLP's genetic material lacking. There are different platforms to produce VLP, among them Baculovirus/insect cell expression system is included. The main advantages of this VLP manufacturing platform are the relatively large amount of correctly assembled VLP in high-density cell culture conditions, ability to scale-up, minimized risk of opportunistic pathogens compared to mammalian cell culture, vaccine adjuvant's properties, associated with low content of host-derived insect cell/baculovirus components, which help trigger an effective immune response. The main disadvantage is that enveloped baculovirus and VLP are produced simultaneously, both share structural similarity (physical and chemical attributes), making purification a tricky and high-cost task (Liu et al., 2013). Approaches based on chromatography techniques have been assessed to solve this issue, among them affinity chromatography proved suitable performance (Moleirinho et al., 2020a). Two insect cell lines are rather used in this platform, *Spodoptera frugiperda* (Sf9) and *Trichoplusia ni* (High Five) cells (Fuenmayor et al., 2017).

Since 2004, when the American Food and Drug Administration's (FDA) launched its guidance on Process Analytical Technology (PAT), the pharmaceutical industry was encouraged to use the innovative tools and technologies to increase understanding and control of manufacturing processes. These include multivariate tools for design, data acquisition and analysis, process analyzers and process control tools (Chew and Sharratt, 2010). Despite their wide use in the chemical industry for decades, their applications within the biopharmaceutical industry have been slower to implement, partly due to the complex matrix background and low concentrations of the molecules of interest. In that sense, spectroscopy technologies such as near-infrared, 2D-fluorescence, and Raman to measure multiple analytes simultaneously in mammalian cell lines have been growing in the scientific literature. Specifically, models based on Raman spectroscopy are scalable and can be used to implement control strategies which improve process performance (Rowland-Jones and Jaques, 2019). Raman spectral data models have found technical feasibility in biopharmaceutical upstream stage since 2011, when several culture parameters (glutamine, glutamate, glucose, lactate, ammonium, viable cell density, and total cell density) for a mammalian cell line were monitored simultaneously for the first time (Abu-Absi et al., 2011). More recently, Raman data modeling has been also applied to insect cell lines (*Spodoptera frugiperda* Sf9 infected by baculovirus), and global models (glucose, lactate) for these parameters demonstrated accuracy regardless of the animal cell line(André et al., 2017a).

The large amount of data generated from spectroscopy analysis of the samples from the biopharmaceutical processes has been processed traditionally by multivariate data analysis (MVDA) to establish correlations between spectral data and critical process and product quality attributes. However, more recently the machine learning has also been used to explore these data. Among MVDA, principal components analysis (PCA) and partial least squares (PLS) have been extensively utilized for this end, when is assumed linear relationships between inputs (spectral data) and responses (monitored parameters) (Banner et al., 2021). PCA has been applied to better understand the root cause of batch-to-batch variations, whereas PLS has been employed for process monitoring and control, as well as for monitoring the end-point quality of fermentations (Banner et al., 2021; Fung Shek and Betenbaugh, 2021). Specifically, PLS has the proven ability to correlate large numbers of spectral data (e.g., spectral wavelengths) with either relevant process or product indicators(Banner et al., 2021).

Thus, this work aimed to calibrate multivariate models from on-line and off-line Raman spectra to quantify growth and biochemical variables (nutrients, metabolites, cell density and viability) in a bioprocess to obtain Rabies virus-like particles using insect cell-baculovirus system. Likely, this work will be a pioneer in using Raman spectroscopy

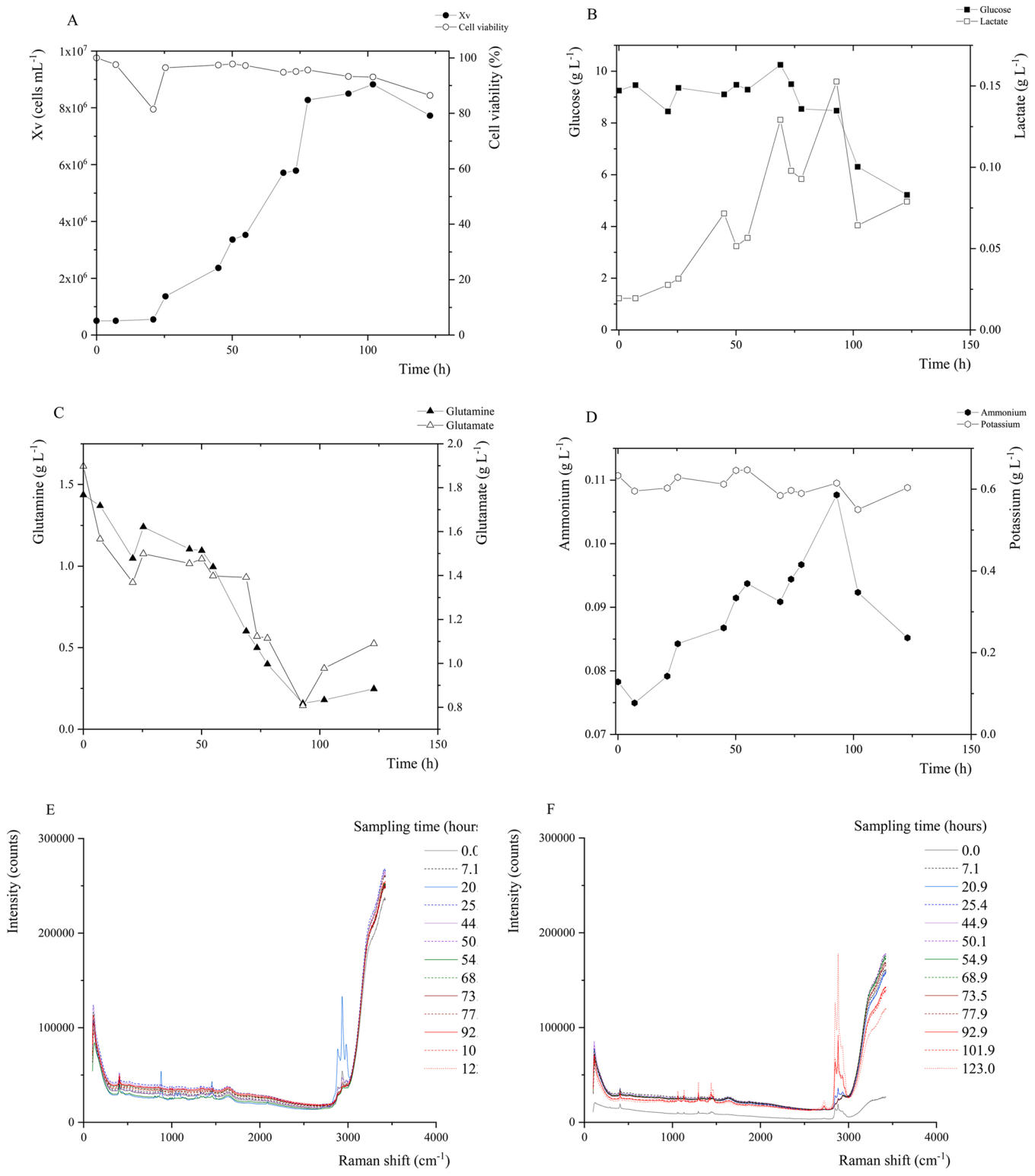

Fig. 1. Primary data from batch experiment for monitoring Sf9 cell growth curve. A: Viable cell density (Xv) and cell viability. B: Glucose and lactate concentrations. C: Glutamine and glutamate concentrations. D: Ammonium and potassium concentrations. E: Average off-line Raman spectral data of each collected sample. F: Average on-line Raman spectral data of each collected sample.

monitoring in insect cell lines throughout all stages of VLP production: cell growth, baculovirus propagation, and VLP expression using global models with minimal experimental data.

2. Materials and methods

2.1. Cell lines and culture media

Sf9 cells in suspension (ATCC 1711) cultivated in serum-free Sf-900^{TM} III serum-free medium (Thermo Fisher Scientific, USA) were

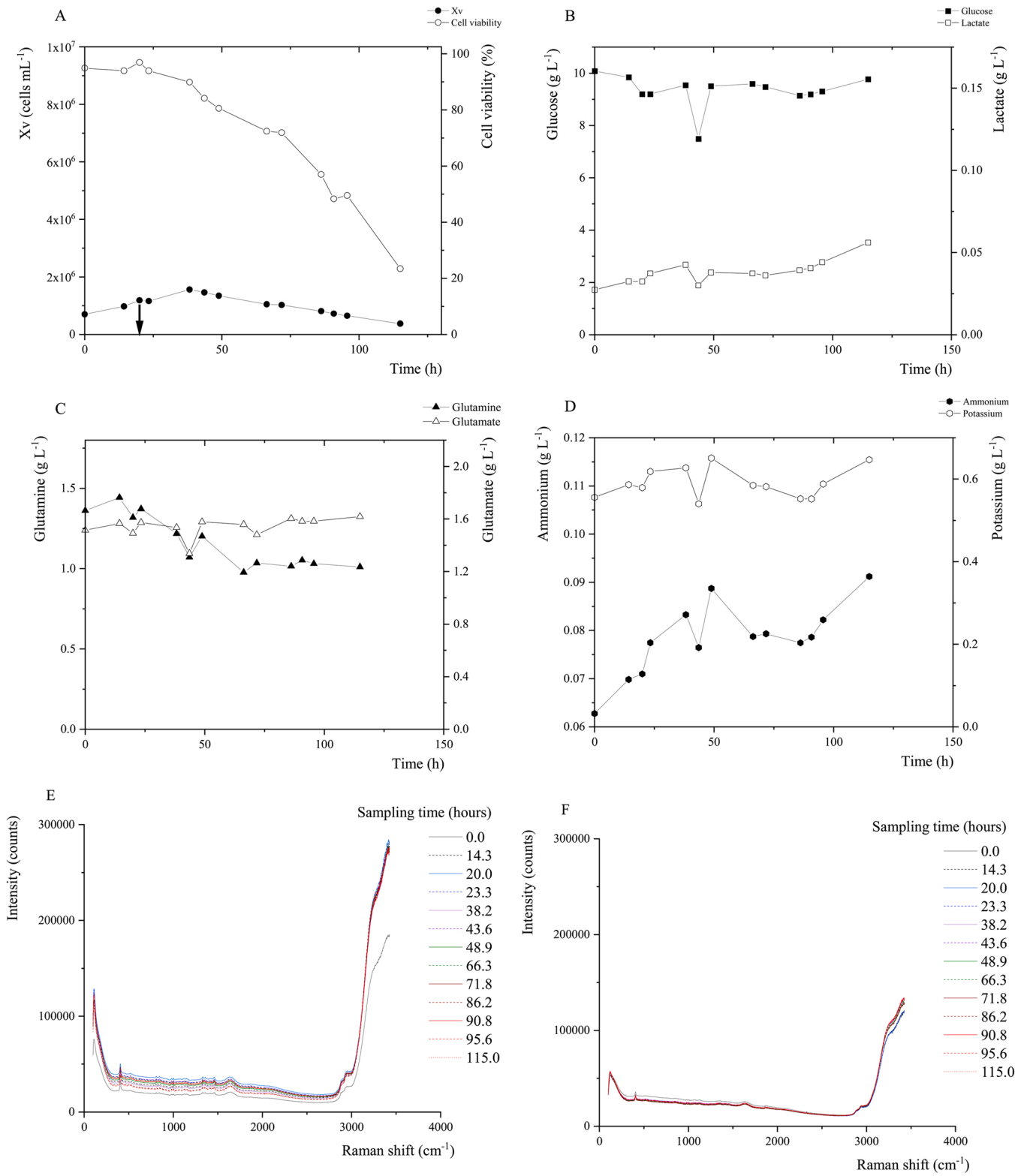

Fig. 2. Primary data from batch experiment for monitoring Sf9 cells coinfected by recombinant baculoviruses bearing rabies virus G glycoprotein and matrix protein at multiplicities of infection of 3 and 2 pfu/cell, respectively. A: Viable cell density (Xv) and cell viability. Black arrow represents the time of infection. B: Glucose and lactate concentrations. C: Glutamine and glutamate concentrations. D: Ammonium and potassium concentrations. E: Average off-line Raman spectral data of each collected sample. F: Average on-line Raman spectral data of each collected sample.

utilized as host for baculovirus propagation and VLP output. The Sf9 ET (Easy Titer) cells, provided kindly by professors Ralph Hopkins and Dominic Esposito from the National Cancer Institute at Frederick (MD, USA), were cultivated in supplemented Sf-900^{TM} III medium with 2.5 % (v/v) fetal bovine serum (FBS, HyClone®, Cytiva, USA) for virus titration. Besides, Sf9 cells were also cultivated in a monolayer over the surface of 25 cm^2 T-flask (Corning Inc.™, Corning, NY, USA) for cell transfection assays.

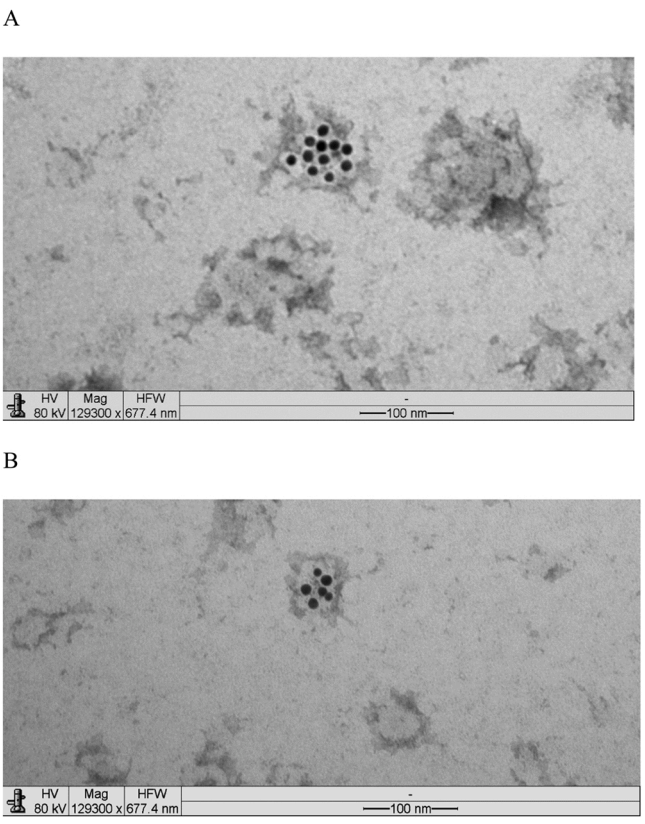

Fig. 3. Transmission electron microscopy of immunolabeled rabies VLP. A: VLP size close to 100 nm (Secondary goat anti-mouse antibody conjugated with 10 nm colloidal gold). B: VLP size around 50 nm (Secondary goat anti-mouse antibody conjugated with 10 nm colloidal gold, and goat anti-rabbit antibody conjugated with 5 nm colloidal gold).

2.2. Viral stock and conservation

Initial viral batches were obtained by transfection of 10 μg of recombinant bacmids (Bac-to-Bac™ Baculovirus Expression System, Gibco/ThermoFisher Scientific, Catalog number: 10359016, CA, USA) bearing rabies virus glycoprotein (RVGP) or matrix protein (RVM) complexed singly each with cationic liposome (Cellfectin II®, Invitrogen, Massachusetts, USA) into 5×10^6 Sf9 cells using a 25 cm^2 T-flask in Sf-900™ III serum-free medium and cultured for 96 h (Bernardino et al., 2021). Then, the supernatant was clarified and stored at 4 °C protected from light, giving rise to passage batch 1. To boost the number of infective baculoviruses used in the infection and co-infection experiments, two consecutive infections were carried out in Schott flasks, with a multiplicity of infection of 0.1 pfu/cell at a cell density of 1×10^6 cells/mL, at 100 rpm rotation speed for 96 h. Both culture supernatants were processed and stored as it was done for obtaining batch 1, and they were identified as batches 2 and 3. No intermediary samples were taken over the assays to obtain batches 1–3.

2.3. Cell inoculum preparation

To get inoculum for the bioreactor, a three passages tandem was completed after a cell vial thawing from a working bank (totaling less than 20 passages since thawing the vial with the cells provided by the ATCC). The initial cell density was within the $0.5–1 \times 10^6$ cells/mL range. The cultures were fulfilled in 100 mL shake flasks (Schott AG™, Mainz, Germany), with 20 mL working volume, in a rotatory incubator shaker (Innova 4000, New Brunswick Scientific, Edison, NJ, USA), at 28°C and 100 rpm orbital shaking.

2.4. Bioreactor experiments

Four batch experiments were carried out in 3 L Bioflo 110 bioreactor (New Brunswick Scientific, Edison, NJ, USA) at 28 °C, using a marine propeller impeller at 80 rpm, with 1 L working volumes. Besides, the dissolved oxygen was set and controlled at 30 % air saturation (Sequeira et al., 2018) by changing the input gas mixture composition. Gas flow was 200 mL/min. Bioflo 110 was connected to a computer with a homemade software implemented in the LabVIEW programming language software (National Instruments, Texas, USA), which records in real time the variables pH, temperature, agitation speed and dissolved oxygen in the medium (DO). The bioreaction time in all experiments was around 122 h (122 ± 5 h, average ± standard deviation). Samples for cell density and viability, metabolism monitoring, recombinant baculovirus titration as well as virus-like particles immunochemical characterization were taken out up to three times daily.

Experiment for noninfected insect cells: Sf9 cells in pre-warmed Sf-900™ III serum-free medium (28 °C) were inoculated to achieve 5×10^5 cells/mL initial density in bioreactor working volume.

Experiment for propagation of the Recombinant baculovirus bearing RVGP (rBV-G): Sf9 cells at 7.4×10^5 cells/mL initial density were infected with rBV-G at 0.1 pfu/cell multiplicity of infection (MOI) at a time of infection (TOI) around 24 h.

Experiments for propagation Recombinant baculovirus bearing RVM (rBV-M): Sf9 cells at 7.2×10^5 cells/mL initial density were infected with rBV-M at 0.1 pfu/cell MOI, at TOI around 36 h. An additional run to propagate rBV-M was included, the cell inoculum was purposefully infected with the recombinant baculovirus to increase sample size and enhance the model's robustness. Thus, leaving the models calibrated to deal with a disturbance that commonly occurs in this type of bioprocess.

Table 2
Comparison among PLS models based on off-line data using different Raman shift ranges (100–3425 cm^{-1}; 400–1850 cm^{-1}; 2800–2425 cm^{-1}); and spectrum filtering approaches (Table 1).

Parameter	100–3425 cm^{-1}			400–1850 cm^{-1}			2800–3425 cm^{-1}		
	Spectra data filtering approach*	Components	RMSEcv	Spectra data filtering approach*	Components	RMSEcv	Spectra data filtering approach*	Components	RMSEcv
Xv (cell/mL)	10	10	1.03E+06	10	12	5.95E+05	8	5	1.61E+06
CV (%)	7	9	19.54	1	10	11.28	3	2	27.63
Gluc (g/L)	7	8	0.74	2	11	0.55	1	3	0.87
Lac (g/L)	2	8	0.01	10	11	0.01	1	5	0.02
Gln (g/L)	8	8	0.19	1	12	0.10	10	3	0.27
Glu (g/L)	10	7	0.15	1	10	0.12	10	4	0.19
NH_4^+ (g/L)	7	8	0.01	1	12	0.01	1	5	0.01
K^+ (g/L)	10	8	0.03	4	6	0.03	NA	-	-

NA: No models could be adjusted, RMSEcv: Root Mean Square Error from cross-validation.
* See Table 1 for identifying the spectral data filtering approach.

Table 3
Comparison among PLS models based on on-line data using different Raman shift ranges (100–3425 cm^{-1}; 400–1850 cm^{-1}; 2800–3425 cm^{-1}); and spectrum filtering approaches (Table 1).

Parameter	100–3425 cm^{-1}			400–1850 cm^{-1}			2800–3425 cm^{-1}		
	Spectra data filtering approach*	Components	RMSEcv	Spectra data filtering approach*	Components	RMSEcv	Spectra data filtering approach*	Components	RMSEcv
Xv (cell/mL)	10	8	9.32E+05	10	11	4.40E+05	10	5	1.15E+06
CV (%)	1	7	14.091	1	10	9.476	1	4	24.654
Gluc (g/L)	1	4	0.599	2	10	0.469	1	2	0.614
Lac (g/L)	1	8	0.015	2	10	0.009	10	3	0.019
Gln (g/L)	1	8	0.145	7	9	0.096	10	5	0.209
Glu (g/L)	1	8	0.150	2	9	0.124	10	3	0.170
NH_4^+ (g/L)	10	8	0.005	10	10	0.004	1	3	0.007
K^+ (g/L)	3	3	0.032	2	8	0.030	1	1	0.034

RMSEcv: Root Mean Square Error from cross-validation.

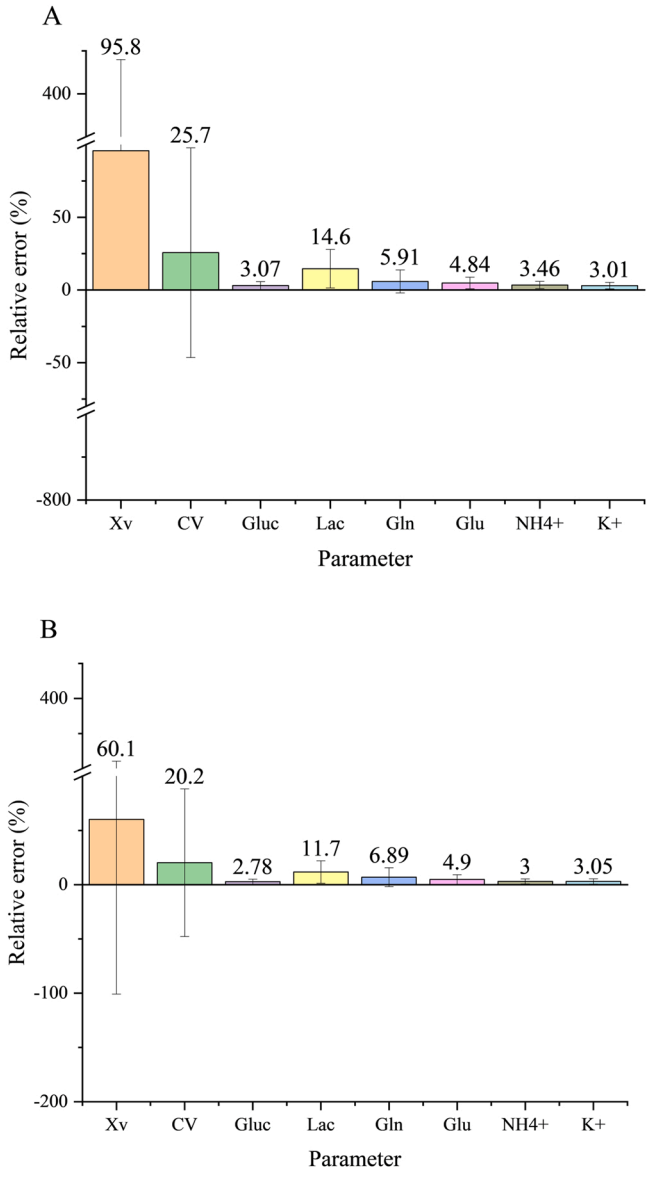

Fig. 4. Relative error average from the best PLS models (400–1850 cm^{-1} range, Tables 1 and 2) for monitored parameters. A: PLS models calibrated from off-line spectral data. B: PLS models calibrated from on-line spectral data. Error Bars represent the standard deviation of Relative error.

Table 4
Comparison of predictive capacity of the best PLS models based on all off-line and on-line data using 400–1850 cm^{-1} Raman shift range. Root Mean Square Error of Prediction (RMSEP) was the prediction index chosen.

Parameter	$RMSEP_{off\text{-}line}$	$RMSEP_{on\text{-}line}$
Xv (cell/mL)	4.08E + 05	5.16E + 05
CV (%)	24.97	13.89
Gluc (g/L)	0.75	0.71
Lac (g/L)	0.01	0.01
Gln (g/L)	0.10	0.12
Glu (g/L)	0.16	0.15
NH_4^+ (g/L)	0.01	0.005
K^+ (g/L)	0.04	0.03

Experiment for obtaining Rabies VLP: Sf9 cells at 5 × 10^5 cells/mL initial cell density were infected simultaneously at TOI around 24 h with rBV-G and rBV-M at MOI of 3 pfu/cell and 2 pfu/cell, respectively. The MOIs choice was based on a work regarding the generation of Rabies VLP holding G and M proteins (Kang et al., 2015).

2.5. Cell density and viability

The cell densities were defined in a light microscope with aid of an improved Neubauer counting chamber (Precicolor, HBG, Giessen-Lützellinden, Germany). Samples were properly diluted with Phosphate Buffer Saline (PBS, 1.76 mM KH_2PO_4, 130 mM NaCl, 2.68 mM KCl, 10.14 mM Na_2HPO_4 - pH 7.0). Cell viability was quantified simultaneously using the trypan blue exclusion method (Augusto et al., 2010).

2.6. Nutrient and metabolite analysis

The cell metabolism throughout the four bioreactions included in this experimental proposal were monitored off-line according to procedures described previously (Núñez et al., 2013). Briefly, five milliliter samples at different times during batches were taken every 12 h. They were centrifuged at 750 x *g* for 4 min. Subsequently, supernants were filtered through 0.22 μm filter and frozen at −20 °C until analysis of nutrients and metabolites.

Glucose, lactate, glutamine and glutamate concentrations from supernatant samples were measured using enzyme-coupled reaction and electrochemical detection, in YSI 2950D-3 Biochemistry Analyzer (YSI Life Sciences, Yellow Springs, OH, USA). Ammonium and potassium were also quantified in the same bioanalyzer using ion selective electrodes (YSI Life Sciences, 2022).

2.7. rBV quantification

The samples with rBVs were titrated using an approach described previously (Hopkins and Esposito, 2009). The procedure is based on the

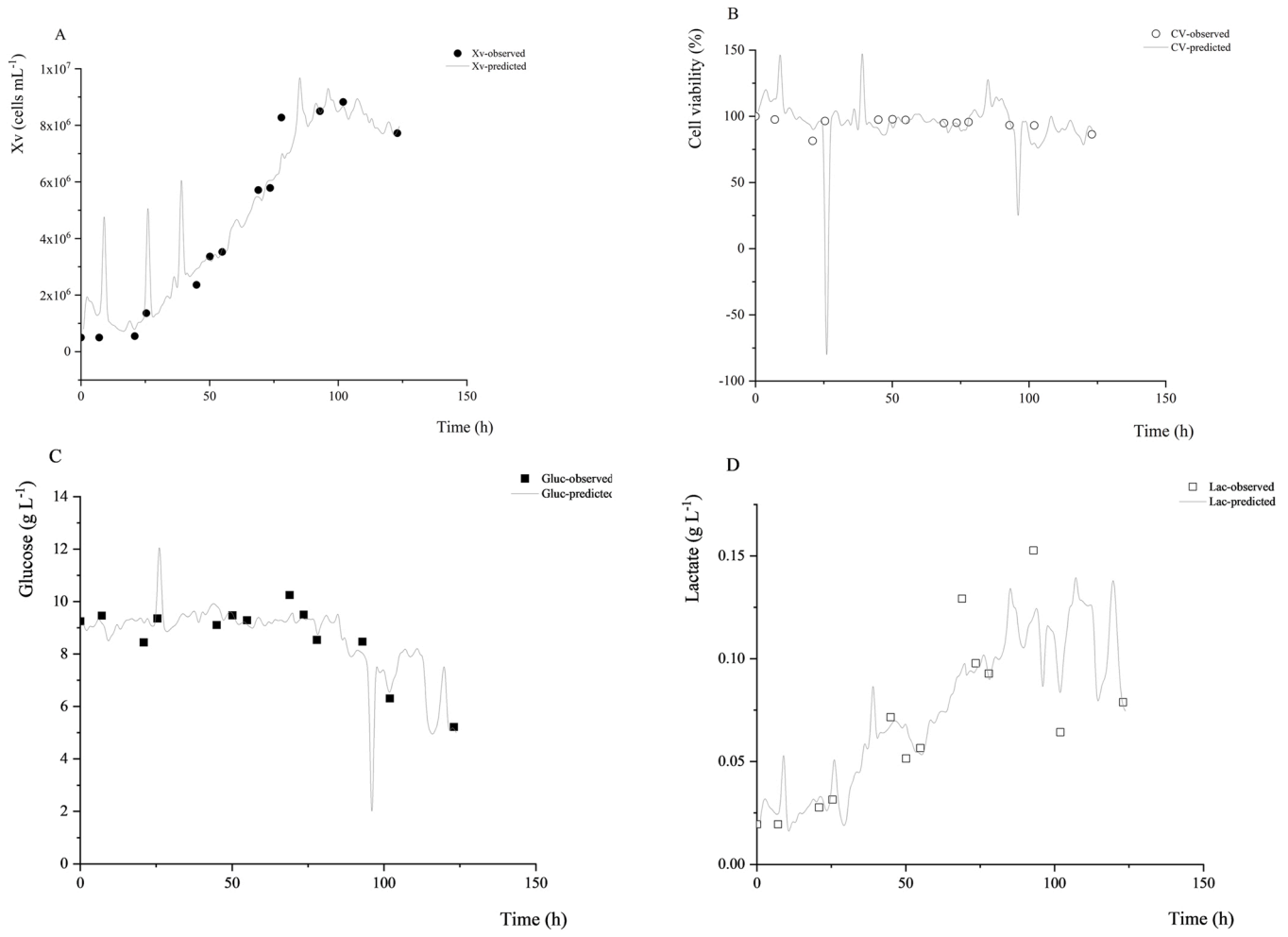

Fig. 5. Comparison between observed (markers) and predicted (line) values of the monitored parameters throughout batch experiment corresponding to Sf9 cell growth curve without infection. Each parameter was predicted every hour using the 6 spectra average. A: Xv; B: CV; C: Gluc; D: Lac; E: Gln; F:Glu; G:NH_4^+; H:K^+.

use of Sf9 ET and virus titer was quantified using a statistical method for calculating median tissue culture infectious dose ($TCID_{50}$) (Reed and Muench, 1938).

2.8. Dot blotting

The primary mouse anti-rabies glycoprotein antibody (LifeSpan BioSciences, LSBio – C75309, Seattle, USA), at a dilution of 1:4000, and the primary rabbit anti-rabies matrix antibody (Cusabio Biotech, CSB-PA322192LA01RAI, Texas, USA) at 1:2000 dilution was used to accomplish the dot blotting assays. As secondary antibodies, the goat HRP anti-mouse antibody (Thermo Fisher Scientific, G21040), at a dilution of 1:4000, and the goat HRP anti-rabbit antibody (Thermo Fisher Scientific, 656120), at a dilution of 1:5000, were used. Briefly, 100 μL of the sample were applied to a nitrocellulose membrane (GE Healthcare Life Science) in the Bio-Dot™ Apparatus device (BioRad, São Paulo, Brazil) and incubated for 90 min in blocking solution (3 % w/v milk skimmed powder in PBS 1x). Then, the membrane was washed with PBS 1x + 0.05 % Tween 20 three times, 10 min each wash. Afterward, the membrane was incubated for 1 h in the corresponding primary antibody and washed three times with PBS 1x + 0.05 % Tween 20. The membrane was immediately incubated with the corresponding secondary antibody for one hour and washed three times with PBS 1x + 0.05 % Tween 20, 10 min each wash. The signal exposure was achieved using the PicoWest SuperSignal Chemiluminescent Substrate kit (Thermo Fisher Scientific), following the manufacturer's recommendations. The images were recorded in the Alliance 2.7 photodocumenter (Uvitec, Cambridge, UK).

Spots' optical densities from dot blot membranes were measured using the Uviband Max software version 1506 (UVITEC Cambridge®, UK). Rabies' matrix protein was quantified by dot blot assay using protein concentration calibration curves (125–2000 ng/mL) also applied to the membranes.

2.9. Enzyme-linked immunosorbent assay (ELISA) for RVGP

A Rabies Glycoprotein Enzyme Immunoassay kit (Pasteur Institute, Paris, France) was used to quantified RVGP by ELISA using a previously described method for insect cell sample treatment (Astray et al., 2008).

2.10. On-line monitoring with Raman spectroscopy and spectral data acquisition

A sterilized stainless-steel immersion probe (12.7 mm diameter) with a sapphire window was installed in Bioflo 110 bioreactor to drive Raman scattering by a fiber optic containing an excitation and collection cable to a multichannel RXN2 Raman spectrometer (Kaiser Optical Systems Inc., KOSI, Ann Arbor, MI, USA) equipped with a 785-nm laser source (around 200 mW power at the sample). The acquisition was made using iCRaman software 4.1 (Mettler Toledo Autochem, Columbia, MD),

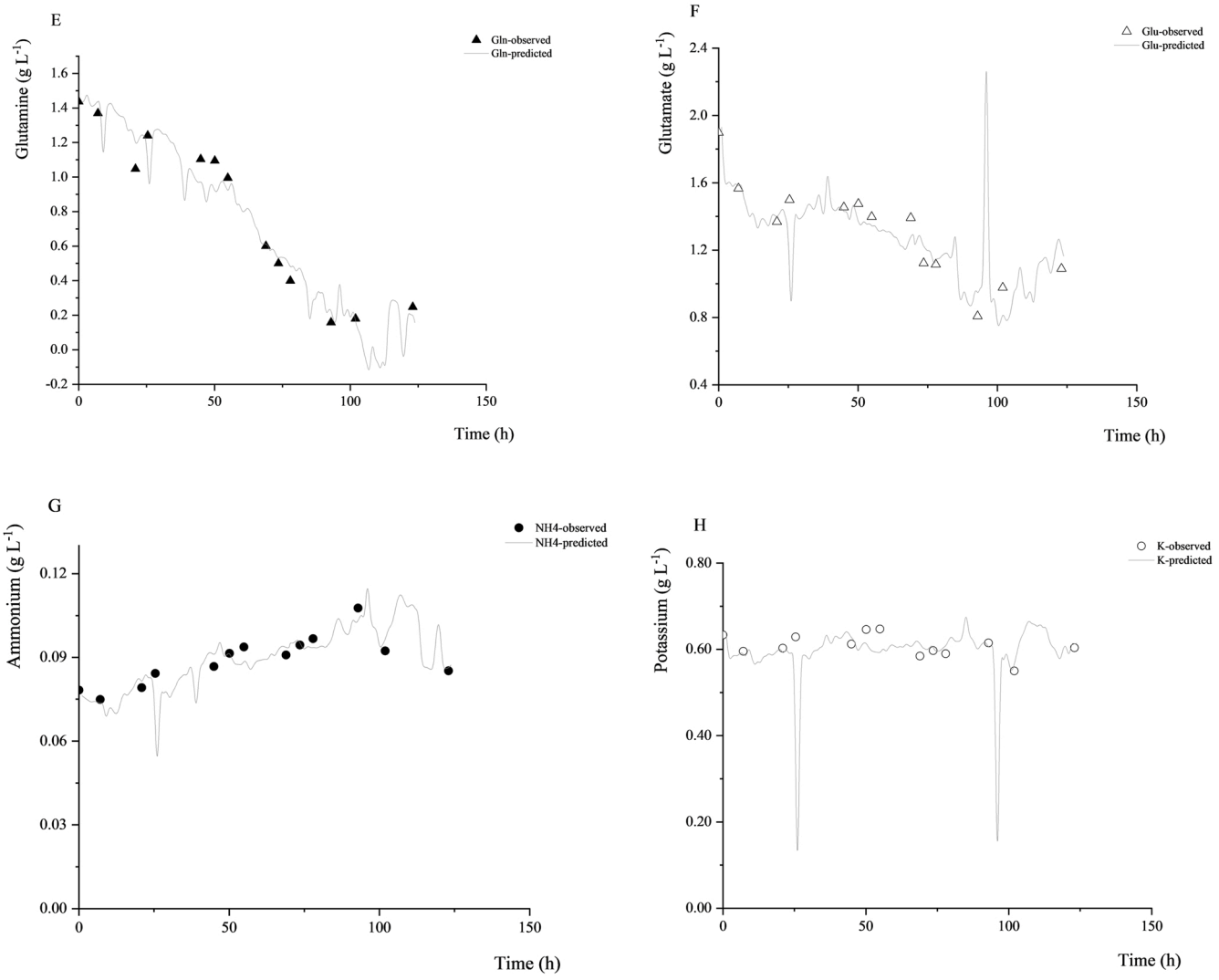

Fig. 5. (*continued*).

considering the selection of cosmic ray removal and dark signal subtraction options. The computers clocks holding the iC Raman software and the homemade software for operating parameters records were synchronized. Spectra were acquired continuously every 30 s, over the 100–3425 cm^{-1} spectral range with a 1 cm^{-1} resolution (André et al., 2017b). The spectra were then exported to Origin 2020 (OriginLab, Northampton, MA, USA) for graphing and further chemometric calculations.

2.11. Off-line monitoring with Raman spectroscopy and spectral data acquisition

Another stainless-steel immersion probe (12.7 mm diameter) with a sapphire window was used to capture off-line Raman spectra using one more of the four channels of the same RXN2 Raman spectrometer. The laser source and power were like those used for on-line Raman spectra acquisitions. After each sample was taken out from the bioreactor, a volume of 8 mL of it, without any processing (containing cells and in some cases recombinant baculovirus and rabies VLP), was placed in contact with the sapphire window of the immersion probe in a dark chamber (centrifuge tube coated with aluminum foil). Six spectra were acquired with 30 s capture time each, over the 100–3425 cm^{-1} spectral range with a 1 cm^{-1} resolution. The off-line Raman models were also assessed to explores the influence of gas bubbles, oxygen concentration, and hydrodynamics of both methods on Raman spectra.

2.12. Transmission electron microscopy

In order to characterize rabies virus-like particles, transmission electron microscopy (TEM) was performed in the Zeiss Leo 906 E device (Electron Microscopy, Germany). Initially, the samples were processed by ultracentrifugation at 150,000 x g for 90 min. The pellet was resuspended in PBS 1 × and passed through a sucrose cushion (20 % w/v) at 230,000 g for 2 h. Then, the new pellet was resuspended in PBS 1 × ; 10 μL of the sample was applied to copper grids pre-coated with parlodium and incubated for 10 min at room temperature. Subsequently, 5 μL of an aqueous solution of 2 % (w/v) uranyl acetate was added and incubated for 1 min. After drying, the grids' micrographs were taken on the electron microscope. For immunostaining of the samples, the primary mouse anti-rabies glycoprotein antibody (LifeSpan BioSciences, LSBio – C75309, Seattle, USA) were used, at a dilution of 1:4000, and the primary rabbit anti-rabies matrix antibody (Cusabio Biotech, CSB-PA322192LA01RAI, Texas, USA) at dilution of 1:2000. Secondary antibodies goat anti-mouse antibody conjugated with 10 nm colloidal gold (ThermoFisher Scientific, A31561, USA) and goat anti-rabbit antibody conjugated with 5 nm colloidal gold (ThermoFisher Scientific, A31565, USA) were used for labeling, both diluted in the proportion of 1:100. The samples were placed in copper grids coated with parlodium and

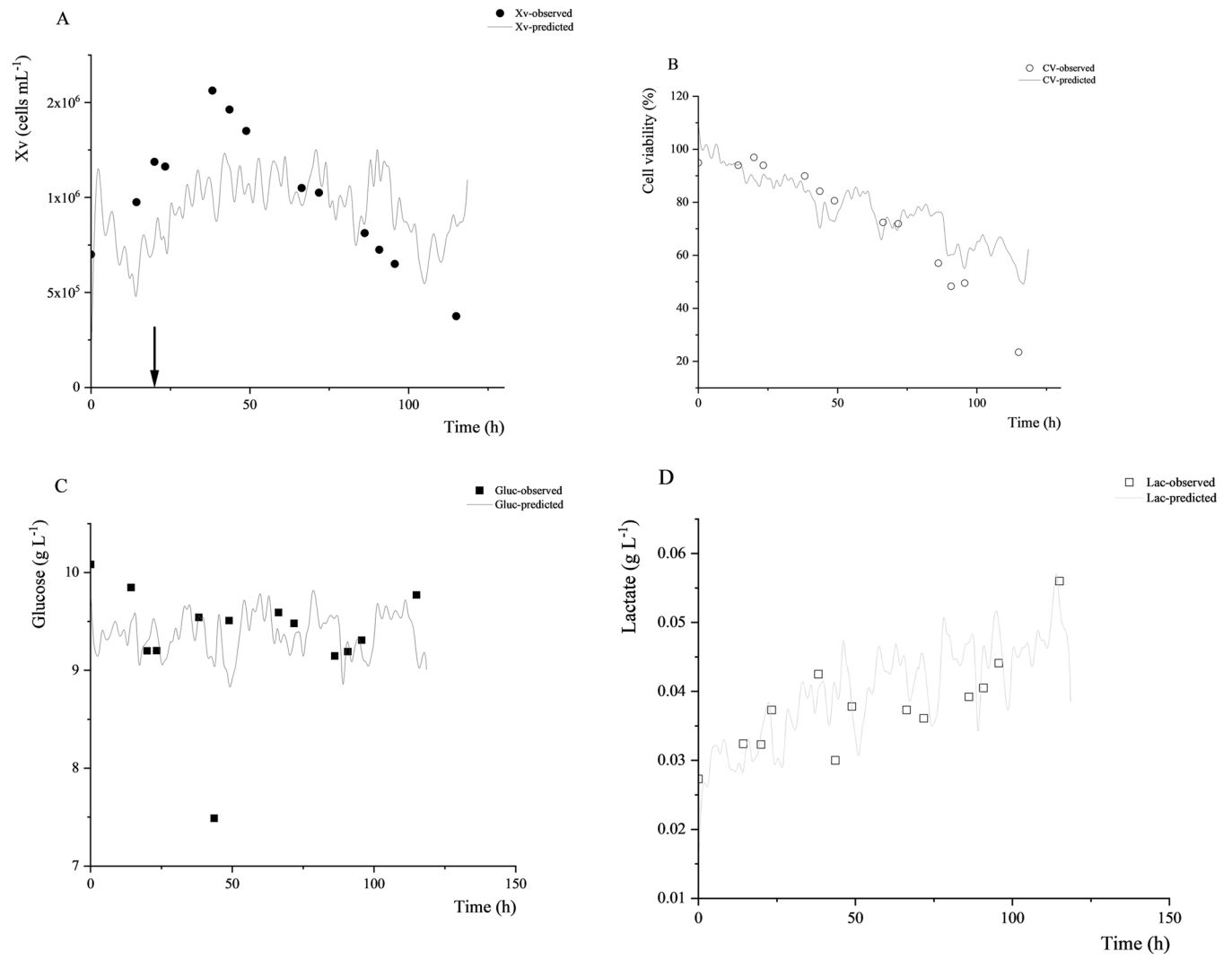

Fig. 6. Comparison between observed (markers) and predicted (line) values of the monitored parameters throughout batch experiment for Sf9 cells coinfected by recombinant baculoviruses bearing rabies virus G glycoprotein and matrix protein at multiplicities of infection of 3 and 2 pfu/cell, respectively. Each parameter was predicted every hour using 6 spectra. A: Xv; B: CV; C: Gluc; D: Lac; E: Gln; F: Glu; G: NH_4^+; H: K^+.

incubated for 15 min. After that, they were incubated for 1 h with the corresponding primary antibody in a dark and humid environment. Then the grids were washed 4 times with PBS 1 × + 1 % BSA, 10 min each wash. Again, they were incubated for 1 h in a humid and dark environment with the corresponding secondary antibody. After that, the grids were washed four times with saline solution (0.9 % w/v NaCl). Finally, the grids were dripped with 10 µL of 2 % uranyl acetate (w/v), and after drying, the samples were observed, and micrographs were taken. For both techniques, the sample magnification used was 129300 X, the accelerating high voltage and horizontal field width (HFW) were 80 kV and 677,4 respectively.

2.13. Statistical analysis

The calibration models were based on Partial Least Squares regression (PLS) and its aim was to calculate latent variables which link the on-line or off-line Raman spectra to the off-line reference measurements of growth and biochemical variables (nutrients, metabolites, cell density and viability). Three Raman shift ranges were assessed (100–3425 cm^{-1}; 400–1850 cm^{-1}; 2800–2425 cm^{-1}) and 10 spectrum filtering approaches were considered before PLS modeling (Table 1). The spectral filtering methods were chosen according to the most frequently used in Raman monitoring in biopharmaceutical applications. To fit and validate models, a cross-validation procedure was implemented using 7 homogeneous groups. The numbers of significant PLS models components (dimensionality) were defined by cross-validation. This approach is useful to handle relatively small databases and achieve reliable models. The best models were chosen based on minimal value of Root Mean Square Error from cross-validation (RMSEcv). The software SIMCA trial version 17 (Sartorius Stedim Data Analytics, Germany) was used for data modeling and prediction. Spectral databases were randomly split into calibration and validation sets, 80 % and 20 %, respectively, multiple times according to cross-validation procedure implemented in SIMCA. The relative error average (e_{r-ave}) between observed and predicted values was calculated according to Eq. 1.

$$e_{r-ave} = \frac{\sum_{i=1}^{N} \frac{|P_{obs} - P_{pred}|}{P_{obs}}}{N} \times 100 \quad (1)$$

N: number of samples in spectral database; P_{obs} : observed parameter value; P_{pred} : predicted parameter value from fitted PLS model.

Root Mean Square Error of Prediction (RMSEP) was used as an index to assess the prediction capacity of the models. RMSEP was calculated from the 20 % of the data set used to validate models, according to the

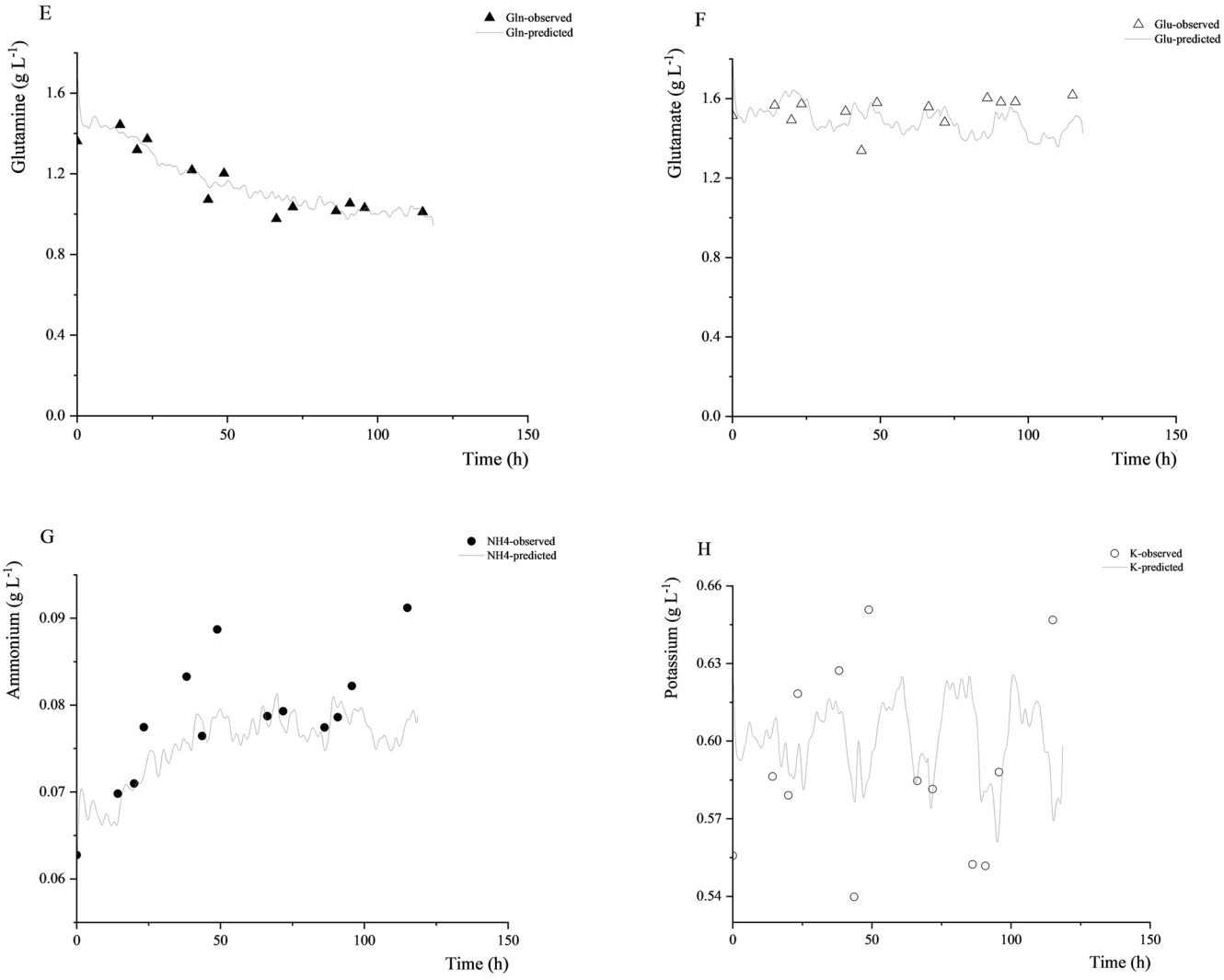

Fig. 6. (*continued*).

Eq. 2.

$$\mathrm{RMSEP} = \sqrt{\frac{\sum \left(P_{obs-v} - P_{pred-v}\right)^2}{n}} \quad (2)$$

n: number of samples included in validation set (20 % of the dataset); P_{obs-v} : observed parameter value for sample included in validation set; P_{pred-v} : predicted parameter value for sample included in validation set.

3. Results and discussion

Raman spectroscopy has intrinsic advantages over other spectroscopic techniques such as near-infrared and infrared in pharmaceutical bioprocess applications due to its specificity, compatibility with aqueous solutions (spectra not sensitive to water), and sampling flexibility. Besides, the proper selection of laser wavelength ensures a maximum Raman signal and minimizes fluorescence (noise) (Lourenço et al., 2012). Raman is useful in understanding composition, molecular structure, and has been used to solve identification, quantification, and process monitoring problems. Spectra from cell cultures and fermentation have a wide and overlapping features. Then, multivariate models and chemometrics tools are recommended to deal with these complex spectral datasets (Esmonde-White et al., 2021). Besides, monitoring techniques based on Raman spectroscopy for pharmaceutical bioprocess have been mainly focused on mammalian cell lines (Rafferty et al., 2020). The current work intended to demonstrate the application of this spectroscopic technique in combination with a multivariate tool to monitor viable cell density, cell viability, glucose, lactate, glutamine, glutamate, ammonium, and potassium in all steps for producing rabies VLP from two monocistronic baculovirus using Sf9 insect cell line as a host.

3.1. Cell performance during growth and infection. Operation parameter monitoring

Viable cell density (Xv), cell viability (CV), glucose (Gluc), lactate (Lac), glutamine (Gln), glutamate (Glu), ammonium (NH_4^+) and potassium (K^+) were monitored in bioreactor assays, in which temperature, dissolved oxygen tension, stirrer speed were controlled at specific values and pH monitored throughout the runs (Supplementary Material: Figs. S1–S3, S5; Figs. 1–2). The assay for describing Sf9 cell growth using Sf900 III culture medium, had a fuzzy control of dissolved oxygen tension at the beginning cause by intermittent blockage of the rotameter used to measure the gas flow (this issue was solved at the end of second culture day) (Supplementary Material: Fig. S1). Other dissolved oxygen tension changes during the five runs occurred due to realization of dynamic method for determination of the specific oxygen consumption rate in each sampling (data not shown) (Supplementary Material:

Figs. S1, S2G, S3G, S4, S5G). The oxygen concentration could affect the PLS model in some extension because this analyte has influence on Raman spectra (Sieburg et al., 2018).

The nutrient consumption and metabolite generation decreased drastically after infection, as well as Xv and CV (Supplementary Material: Figs. S2, S3, S5; Figs. 1–2). These events were associated to increase of viral titer and VLP production (Supplementary Material: Figs. S6, S7). The expression yields obtained herein for the rabies VLP (2.8 mg/L G-glycoprotein and 1.1 mg/L M-protein by DOT;) are within the range (0.2–662 mg/L) for other VLP licensed or in an advanced stage of development (Vicente et al., 2011). The rabies VLP during the coinfection were in a 50–100 nm size range (Fig. 3). The decrease of glucose and glutamine specific consumption rates, as well as no utilization of glutamate after baculovirus infection in Sf9 cell line with respect to equivalent values for Sf9 cell growth without infection, have already been reported (Wong et al., 1994). However, the observed analytes concentration oscillations after virus infection could be associated with baculovirus lytic cycle. The replacement of nutrients and increase in metabolite concentrations could be due to cellular breakdown during virus release. The virus titer profiles showed an exponential propagation pattern, common for this platform (baculovirus/insect cells) (Power et al., 1992). However, the assay that was infected from the beginning of the cell culture did not show this pattern, likely, because of the low cell density at TOI.

3.2. Raman spectral data and modeling

The spectral data among samples showed pronounced alterations in 400–1850 cm^{-1} and 2800–3425 cm^{-1} Raman shift ranges (Supplementary Material: Figs. S2, S3, S5; Figs. 1–2). These spectral regions are rich in organic compounds fingerprints (Rafferty et al., 2020). The parameter profiles were different for the run using only Sf9 cells and those related to infection processes. The Raman shift range and spectrum filtering approach to calibrate PLS models for monitored parameters showed a significant impact on their predictive capacity (Tables 2–3). The best Raman shift range was 100–1850 cm^{-1}, both off-line and on-line acquired spectra. However, there was not a single filtering approach suitable for all parameters under consideration. Row-center baseline correction in combination with standard normal variate (SNV) and multiplicative signal correction (MSC) as well as the united use of lowest offset baseline correction and SNV were the filtering strategies, which found more application in off-line data. Besides, the lowest offset baseline correction in combination with SNV and multiplicative signal correction (MSC) was the most common filtering approach for on-line data.

The 100–1850 cm^{-1} Raman signal range comprises molecule fingerprints for glucose, lactate, glutamine, glutamate, and potassium salts (Santos et al., 2018; Shurvell and Bergin, 1989; Willis et al., 2008). This seems to explain the best fitting of PLS models to the observed parameter values. However, ammonium gives a signature at about 2800 cm^{-1} (Fontana et al., 2013). The use of the spectrum sections defined above was also to avoid lambda region (where the two spectra are joined in each spectrum) and capture the C-H stretching section (Rafferty et al., 2020).

The model relative error was similar for on-line and off-line spectral data for nutrients, metabolites, and CV, most of them below 10 %. However, the Xv models based on on-line and off-line spectra showed high relative error (Fig. 4). Its worthy to highlight that Xv models for recombinant mammalian cell line culture based on Raman spectral data did not perform either well, with a relative error of 36.3 %, suggesting Raman spectroscopy is not able of distinguishing between live and dead cells (Whelan et al., 2012). Xv could be more difficult to model properly in viral infection processes because the sample chemical background changes drastically even for similar Xv values (before and after infection). Besides, the RMSEP for lactate and ammonium of off-line and on-line PLS models (Table 4) were lower than those reported for Chinese hamster ovary cells (Rafferty et al., 2020).

3.3. Real-time and off-line prediction of biochemical parameters

The model fittings from on-line spectra to the experimental data was also confirmed using acquired spectra every hour after cell inoculation. As a rule, parameters profile showed smooth pattern in correspondence to the experimental data and their own expected kinetic curve. At some points, like the beginning Sf9 cell growth experiment without infection and others when specific oxygen consumption rate was being determined, a noise could be observed. This fact seems to be associated with sporadic poor control of dissolved oxygen tension, which impacts Raman spectra (Figs. 5–6; Supplementary Material: Figs. S8–S10) (Ganoe and DeYoung, 2013). The models developed in this work intended to use minimal experimental data to predict main nutrients and metabolites concentration, as well as growth parameters throughout all stages of rabies VLP production. Thus, the viable cell density and cell viability were the predicted parameters with less accuracy. This finding could be justified based on the same values of these parameters can be quantified in cell growth and infection assays with quite different chemical backgrounds. Non-linear models, such as the artificial neural networks models could be explored in the future to improve the prediction quality of viable cell densities and cell viability. The on-line Raman models could be useful to implement fed-batch strategies throughout all upstream steps for producing rabies VLP in order to improve the bioprocess performance.

Once calibrated PLS models for growth and biochemical parameters from off-line Raman spectral data can significantly be reduced the time of sample quantifications, delay in issuing results from sampling moment, labor, and reagent costs because all parameters will be determined simultaneously in around 1 min without previous sample preparation. However, the operator should take some care such as shake the sample to avoid cell settling before spectra acquisitions and to perform the spectral reading as soon as possible the sample is taken out to ensure minimal changes in the desired parameters and to keep the temperature close to 28ºC. Specifically, Raman spectrum is sensitive to temperature (Lin et al., 2021). Besides, the current high cost of Raman spectroscopy equipment is one of the major hurdles to introduce it in biopharmaceutical routines labs. Nevertheless, the cost of Raman spectroscopy is expected to decrease in the years ahead, so this technique will become more accessible in biologicals industry (Lin et al., 2021). The off-line Raman models could be used to monitor biochemically all development stages of this rabies VLP production platform, thereby improving process characterization and optimization.

4. Conclusions

The current work demonstrated the suitability of Raman spectroscopy for monitoring baculovirus/insect cell system aiming Sf9 cell growth, baculovirus propagation and virus-like particles production. On-line and off-line data allowed for partial least squares modelling satisfactorily nutrients (glucose, glutamine, glutamate, potassium) and metabolites (lactate, ammonium); the relative error was less than 15 %. However, the use of this chemometrics approach for viable cell density and cell viability was not as accurate as it was for the above-mentioned parameters. Even so, the models herein could be used during the following stages of upstream development for rabies virus-like particles as well as to perform metabolic studies with robustness.

CRediT authorship contribution statement

Luis Giovani Oliveira Guardalini: Conceptualization, methodology, experimental tasks, manuscript writing; **Paulo Eduardo da Silva Cavalcante**: experimental tasks; **Jaci Leme**: experimental tasks; **Renata Gois de Mello**: experimental tasks; **Thaissa Consoni Bernardino**: experimental tasks, manuscript edition; **Renato Mancini Astray**:

Conceptualization, methodology, manuscript edition; **Eduardo Barbosa**: Conceptualization, methodology, manuscript edition; **Suellen Regina da Silveira**: Conceptualization, methodology; **Paulo Lee Ho**: Conceptualization, methodology, manuscript edition, **Aldo Tonso**: Conceptualization, methodology, data curation, manuscript edition; **Soraia Attie Calil Jorge**: Conceptualization, methodology, manuscript edition; **Eutimio Gustavo Fernández Núñez**: Conceptualization, methodology, modeling and statistical analysis, manuscript writing.

Declaration of Competing Interest

The authors declare that they have no known competing financial interests or personal relationships that could have appeared to influence the work reported in this paper.

Data availability

Data will be made available on request.

Acknowledgements

This work was financially supported by Pensalab Equipamentos Industriais S.A. (Installation and temporary availability of KOSI Raman spectrometer), the National Council of Technological and Scientific Development (CNPq) (grant numbers 168539/2018-7 and 401346/2020-0), the São Paulo Research Foundation (FAPESP) (grants no. 16/22780-6, no. 2018/10538-1) and Butantan Foundation. The research team acknowledges Marta Maria Antoniazzi and Simone Gonçalves Silva Jared for their valuable support in Transmission Electron Microscopy, as well as Laboratory of Viral Vaccine staff from Butantan Institute for backing in the biochemical assays. The corresponding author is very grateful to his wife, Relma, and daughters, Giovanna and Paola, for their significant support in writing this manuscript.

Appendix A. Supporting information

Supplementary data associated with this article can be found in the online version at doi:10.1016/j.jbiotec.2022.12.009.

References

Abu-Absi, N.R., Kenty, B.M., Cuellar, M.E., Borys, M.C., Sakhamuri, S., Strachan, D.J., Hausladen, M.C., Li, Z.J., 2011. Real time monitoring of multiple parameters in mammalian cell culture bioreactors using an in-line Raman spectroscopy probe. Biotechnol. Bioeng. 108, 1215–1221. https://doi.org/10.1002/bit.23023.

André, S., Lagresle, S., Da Sliva, A., Heimendinger, P., Hannas, Z., Calvosa, É., Duponchel, L., 2017a. Developing global regression models for metabolite concentration prediction regardless of cell line. Biotechnol. Bioeng. 114, 2550–2559. https://doi.org/10.1002/bit.26368.

André, S., Lagresle, S., Hannas, Z., Calvosa, É., Duponchel, L., 2017b. Mammalian cell culture monitoring using in situ spectroscopy: Is your method really optimised? Biotechnol. Prog. 33, 308–316. https://doi.org/10.1002/btpr.2430.

Astray, R.M., Augusto, E., Yokomizo, A.Y., Pereira, C.A., 2008. Analytical approach for the extraction of recombinant membrane viral glycoprotein from stably transfected Drosophila melanogaster cells. Biotechnol. J. 3, 98–103. https://doi.org/10.1002/biot.200700179.

Augusto, E.F.P., Moraes, A.M., Piccoli, R.A.M., Barral, M.F., Suazo, C.A.T., Tonso, A., Pereira, C.A., 2010. Nomenclature and guideline to express the amount of a membrane protein synthesized in animal cells in view of bioprocess optimization and production monitoring. Biologicals 38, 105–112. https://doi.org/10.1016/j.biologicals.2009.07.005.

Banner, M., Alosert, H., Spencer, C., Cheeks, M., Farid, S.S., Thomas, M., Goldrick, S., 2021. A decade in review: use of data analytics within the biopharmaceutical sector. Curr. Opin. Chem. Eng. 34, 100758 https://doi.org/10.1016/j.coche.2021.100758.

Bernardino, T.C., Astray, R.M., Pereira, C.A., Boldorini, V.L., Antoniazzi, M.M., Jared, S. G.S., Núñez, E.G.F., Jorge, S.A.C., 2021. Production of rabies VLPs in insect cells by two monocistronic baculoviruses approach. Mol. Biotechnol. https://doi.org/10.1007/s12033-021-00366-z.

Chew, W., Sharratt, P., 2010. Trends in process analytical technology. Anal. Methods 2, 1412. https://doi.org/10.1039/c0ay00257g.

Esmonde-White, K.A., Cuellar, M., Lewis, I.R., 2021. The role of Raman spectroscopy in biopharmaceuticals from development to manufacturing. Anal. Bioanal. Chem. https://doi.org/10.1007/s00216-021-03727-4.

Fontana, M.D., Ben Mabrouk, K., Kauffmann, T.H., 2013. Raman spectroscopic sensors for inorganic salts. In: Yarwood, J., Douthwaite, R., Duckett, S. (Eds.), Spectroscopic Properties of Inorganic and Organometallic Compounds. RSCPublishing, pp. 40–67. https://doi.org/10.1039/9781849737791-00040.

Fooks, A.R., Banyard, A.C., Ertl, H.C.J., 2019. New human rabies vaccines in the pipeline. Vaccine 37, A140–A145. https://doi.org/10.1016/j.vaccine.2018.08.039.

Fuenmayor, J., Gòdia, F., Cervera, L., 2017. Production of virus-like particles for vaccines. N. Biotechnol. 39, 174–180. https://doi.org/10.1016/j.nbt.2017.07.010.

Fung Shek, C., Betenbaugh, M., 2021. Taking the pulse of bioprocesses: at-line and in-line monitoring of mammalian cell cultures. Curr. Opin. Biotechnol. 71, 191–197. https://doi.org/10.1016/j.copbio.2021.08.007.

Ganoe, R., DeYoung, R., 2013. Remote sensing of dissolved oxygen and nitrogen in water using Raman spectroscopy. National Aeronautics and Space Administration, Langley Research Center, Virginia.

Hopkins, R.F., Esposito, D., 2009. A rapid method for titrating baculovirus stocks using the Sf-9 Easy Titer cell line. Biotechniques 47, 785–788. https://doi.org/10.2144/000113238.

Kang, H., Qi, Y., Wang, H., Zheng, X., Gao, Y., Li, N., Yang, S., Xia, X., 2015. Chimeric rabies virus-like particles containing membrane-anchored GM-CSF enhances the immune response against rabies virus. Viruses 7, 1134–1152. https://doi.org/10.3390/v7031134.

Kesik-Brodacka, M., 2018. Progress in biopharmaceutical development. Biotechnol. Appl. Biochem. 65, 306–322. https://doi.org/10.1002/bab.1617.

Lin, Y.K., Leong, H.Y., Ling, T.C., Lin, D.-Q., Yao, S.-J., 2021. Raman spectroscopy as process analytical tool in downstream processing of biotechnology. Chin. J. Chem. Eng. 30, 204–211. https://doi.org/10.1016/j.cjche.2020.12.008.

Liu, F., Wu, X., Li, L., Liu, Z., Wang, Z., 2013. Use of baculovirus expression system for generation of virus-like particles: successes and challenges. Protein Expr. Purif. 90, 104–116. https://doi.org/10.1016/j.pep.2013.05.009.

Lourenço, N.D., Lopes, J.A., Almeida, C.F., Sarraguça, M.C., Pinheiro, H.M., 2012. Bioreactor monitoring with spectroscopy and chemometrics: a review. Anal. Bioanal. Chem. 404, 1211–1237. https://doi.org/10.1007/s00216-012-6073-9.

McKenzie, E.A., Abbott, W.M., 2018. Expression of recombinant proteins in insect and mammalian cells. Methods 147, 40–49. https://doi.org/10.1016/j.ymeth.2018.05.013.

Moleirinho, M.G., Fernandes, R.P., Carvalho, S.B., Bezemer, S., Detmers, F., Hermans, P., Silva, R.J.S., Alves, P.M., Carrondo, M.J.T., Peixoto, C., 2020a. Baculovirus affinity removal in viral-based bioprocesses. Sep. Purif. Technol. 241, 116693 https://doi.org/10.1016/j.seppur.2020.116693.

Moleirinho, M.G., Silva, R.J.S., Alves, P.M., Carrondo, M.J.T., Peixoto, C., 2020b. Current challenges in biotherapeutic particles manufacturing. Expert Opin. Biol. Ther. 20, 451–465. https://doi.org/10.1080/14712598.2020.1693541.

Moraes, Â.M., Jorge, S.A.C., Astray, R.M., Suazo, C.A.T., Calderón Riquelme, C.E., Augusto, E.F.P., Tonso, A., Pamboukian, M.M., Piccoli, R.A.M., Barral, M.F., Pereira, C.A., 2012. Drosophila melanogaster S2 cells for expression of heterologous genes: from gene cloning to bioprocess development. Biotechnol. Adv. 30, 613–628. https://doi.org/10.1016/j.biotechadv.2011.10.009.

Núñez, E.G.F., Leme, J., de Almeida Parizotto, L., Chagas, W.A., de Rezende, A.G., da Costa, B.L.V., Monteiro, D.C.V., Boldorini, V.L.L., Jorge, S.A.C., Astray, R.M., Pereira, C.A., Caricati, C.P., Tonso, A., 2013. Influence of aeration–homogenization system in stirred tank bioreactors, dissolved oxygen concentration and pH control mode on BHK-21 cell growth and metabolism. Cytotechnology. https://doi.org/10.1007/s10616-013-9612-0.

Orphanou, C., Gervais, D., 2018. Higher-order structure and conformational change in biopharmaceuticals. J. Chem. Technol. Biotechnol. 93, 2477–2485. https://doi.org/10.1002/jctb.5682.

Power, J., Greenfield, P.F., Nielsen, L., Reid, S., 1992. Modelling the growth and protein production by insect cells following infection by a recombinant baculovirus in suspension culture. Cytotechnology 9, 149–155. https://doi.org/10.1007/BF02521742.

Rafferty, C., Johnson, K., O'Mahony, J., Burgoyne, B., Rea, R., Balss, K.M., 2020. Analysis of chemometric models applied to Raman spectroscopy for monitoring key metabolites of cell culture. Biotechnol. Prog. 36. https://doi.org/10.1002/btpr.2977.

Reed, L.J., Muench, H., 1938. A simple method of estimating fifty per cent endpoints. Am. J. Epidemiol. 27, 493–497. https://doi.org/10.1093/oxfordjournals.aje.a118408.

Riccardi, N., Giacomelli, A., Antonello, R.M., Gobbi, F., Angheben, A., 2021. Rabies in Europe: an epidemiological and clinical update. Eur. J. Intern. Med. 88, 15–20. https://doi.org/10.1016/j.ejim.2021.04.010.

Rowland-Jones, R.C., Jaques, C., 2019. At-line raman spectroscopy and design of experiments for robust monitoring and control of miniature bioreactor cultures. Biotechnol. Prog. 35, e2740 https://doi.org/10.1002/btpr.2740.

Rüdt, M., Vormittag, P., Hillebrandt, N., Hubbuch, J., 2019. Process monitoring of virus-like particle reassembly by diafiltration with UV/Vis spectroscopy and light scattering. Biotechnol. Bioeng. 116, 1366–1379. https://doi.org/10.1002/bit.26935.

Santos, R.M., Kessler, J.-M., Salou, P., Menezes, J.C., Peinado, A., 2018. Monitoring mAb cultivations with in-situ raman spectroscopy: the influence of spectral selectivity on calibration models and industrial use as reliable PAT tool. Biotechnol. Prog. 34, 659–670. https://doi.org/10.1002/btpr.2635.

Sequeira, D.P., Correia, R., Carrondo, M.J.T., Roldão, A., Teixeira, A.P., Alves, P.M., 2018. Combining stable insect cell lines with baculovirus-mediated expression for multi-HA influenza VLP production. Vaccine 36, 3112–3123. https://doi.org/10.1016/j.vaccine.2017.02.043.

Shurvell, H.F., Bergin, F.J., 1989. Raman spectra of L(+)-glutamic acid and related compounds. J. Raman Spectrosc. 20, 163–168. https://doi.org/10.1002/jrs.1250200307.

Sieburg, A., Schneider, S., Yan, D., Popp, J., Frosch, T., 2018. Monitoring of gas composition in a laboratory biogas plant using cavity enhanced Raman spectroscopy. Analyst 143, 1358–1366. https://doi.org/10.1039/C7AN01689A.

Starodubova, E.S., Preobrazhenskaia, O.V., Kuzmenko, Y.V., Latanova, A.A., Yarygina, E. I., Karpov, V.L., 2015. Rabies vaccines: Current status and prospects for development. Mol. Biol. 49, 513–519. https://doi.org/10.1134/S0026893315040172.

Vicente, T., Roldão, A., Peixoto, C., Carrondo, M.J.T., Alves, P.M., 2011. Large-scale production and purification of VLP-based vaccines. J. Invertebr. Pathol. 107, S42–S48. https://doi.org/10.1016/j.jip.2011.05.004.

Whelan, J., Craven, S., Glennon, B., 2012. In situ Raman spectroscopy for simultaneous monitoring of multiple process parameters in mammalian cell culture bioreactors. Biotechnol. Prog. 28, 1355–1362. https://doi.org/10.1002/btpr.1590.

Willis, L.B., Gil, G.A., Lee, H.L., Choi, D., Schoenheit, J., Ram, R.J., Rha, C., Sinskey, A.J., 2008. Application of spectroscopic methods for the automation of oil palm culture. J. Oil Palm. Res 1, 1–13.

Wong, T.K.K., Nielsen, L.K., Greenfield, P.F., Reid, S., 1994. Relationship between oxygen uptake rate and time of infection of Sf9 insect cells infected with a recombinant baculovirus. Cytotechnology 15, 157–167. https://doi.org/10.1007/BF00762390.

YSI Life Sciences, 2022. YSI 2900 Series Biochemistry Analyzers [WWW Document]. Brochure-B51 713. URL ⟨https://www.xylem.com/siteassets/brand/ysi/resources/brochure/ysi-2900-series-analyzer-brochure-b51.pdf⟩ (accessed 9.25.22).